Experimental Study on the Burning Characteristics of Transformer Oil Pool Fires

Combustion

Experimental study on the burning characteristics of transformer oil pool fires

Jinlong Zhao, Wang Shansheng, Jianping Zhang, Rui Zhou, and Rui Yang

Energy Fuels, **Just Accepted Manuscript** • DOI: 10.1021/acs.energyfuels.0c00175 • Publication Date (Web): 16 Mar 2020

Experimental study on the burning characteristics of transformer oil pool fires

Jinlong Zhao[a,b*], Shansheng Wang[a], Jianping Zhang[b], Rui Zhou[c] , Rui Yang[c]

a. School of Emergency Management & Safety Engineering, China University of Mining & Technology, Beijing, China

b. FireSERT, Belfast School of Architecture and the Built Environment, Ulster University, Newtownabbey, BT37 0QB, United Kingdom

c. Institute of Public Safety Research, Department of Engineering Physics, Tsinghua University, Beijing, China

ABSTRACT: This paper examines experimentally the burning behaviors of transformer oil pool fires. A series of transformer oil pool fire tests with different pool diameters (0.2~1m) was conducted. The mass burning rate, flame height, liquid layer temperature, flame temperature, and radiative heat flux were measured and analyzed. A new correlation for the mass burning rate as a function of pool diameter is deduced. The experimental flame height is compared to existing correlations and it is found that the present result is in better agreement with those deduced for heavy oils. The liquid temperature results show that the fuel layer consists of a boiling layer and a gradient layer, and the thickness of the boiling layer is found to be around 2.6 mm independent of the pool diameter. The flame temperature is also analyzed and three zones are observed, for which a piecewise function is deduced. The radiation fraction and the emissive power of the flame are determined respectively based on the source flame model and solid flame model, and an exponential decay of the radiation fraction as a function of pool diameter is obtained. The present results are important for estimation of thermal radiation from a pool fire on the surrounding objects in practical transformer oil fires.

Key Words: transformer fires; burning rate; flame height; temperature profile; radiation

1. INTRODUCTION

A wide variety of oil-immersed transformers is commonly used in electrical power delivery networks[1]. During the conversion of voltage, heat will be produced, and the transformer oil is usually used to cool down the transformers [2]. As transformer oils are highly flammable, fire accidents or even boil-over can be triggered by external conditions, such as lightning strikes, switching transients, short-circuits, or other incidents[1]. The common probability of (0.04~0.25)% per year was used in the fire hazard analysis[3]. The development of transformer fire accidents was categorized into four stages: arc forming, oil pyrolysis, overpressure and equipment cracking[4]. After the cracking, the oil will overflow under gravity and then form a large burning area in the oil pit, which poses a great hazard to the nearby persons and equipment. This has been demonstrated in a serious transformer oil fire accident that occurred in December 22, 2019 in Jinan (a Chinese city)[5]. It was reported that the transformer oil leaked from the box and then formed a pool fire accident after the deflagration, which resulted in one fatality and two injuries[5].

The transformer fire hazard is closely associated with the transformer oil burning characteristics[6]. There has been considerable research describing the burning behaviors of hydrocarbon fuels, including heat feedback[7], mass burning rate[8,9], flame height[10], etc. The mass burning rate, as one of the key parameters, depends on the pool size through a change of heat feedback from the flame to the fuel surface[7]. The heat feedback mechanism has been categorized into three regimes: conduction controlled (D<0.1m), convection controlled (0.1m<D<0.2m) and radiation controlled (D>0.2m)[9,11]. In practical fire accidents, the burning is usually controlled by radiation due to their large pool diameters. Burgess et al.[11] derived an empirical correlation to calculate the burning rate of a pool fire ($m_\infty(1-e^{-k\beta D})$ for large-scale burning, where m_∞ is the mass burning rate of an infinite pool diameter; $k\beta$ is a constant for fuels; D is the burning diameter). Subsequently Babrauskas[9] provided the detail values ($m_\infty, k\beta$) for some fuels, including those of the transformer oil (m_∞ =0.039g/(m^{2}s), $k\beta$=0.7m^{-1})[12]. These values have been widely used in some applications[13, 14,] however it is important to note that they were derived from

experimental data with only two pool diameters (D=1.2m and D=1.7m) for transformer oil pool fires[9]. In recent years, the values of m_∞ and $k\beta$ have been constantly updated with new experimental data for some fuels, such as gasoline and kerosene[8,13], however these for transformer oils have not been due to a lack of experimental data. Therefore the burning rate as a function of pool diameter for transformer oil is still unclear and needs to be further examined given its importance in the determination of flame height, radiation fraction and other important combustion characteristics such as heat release rate and flame temperature and velocities[10,16,17].

To date, the research on transformer oil pool fires is relatively limited, particularly using systematic experiments. Heskestad and Dobson[17] conducted pool fire experiments using transformer oil over a rock bed in a 1.2 m diameter pan with and without drainage at the bottom of the pan and found that the fires self-extinguished after the liquid level decreased to a critical value in the drainage experiments. Zhang et al.[6] conducted pool fire experiments using a cone calorimeter under five external radiative heat fluxes using three types of transformer oils (10#, 25# and 45#) and found that the ignition time of transformer oil decreased exponentially with the increase of heat fluxes. In addition, the effects of the thickness of transformer oil on the ignition characteristics were also discussed in the paper[18]. Wang et al.[19] performed experiments on the auto-ignition characteristics of pure and oil-impregnated transformer insulating paper board and analyzed the ignition time, heat release rate and gas concentrations during fuel burning. It is worthwhile to note that in these studies[6,18-19,] the equivalent diameter of the fire ($\sqrt{4S/\pi}$, where S is the pool area) is all less than 10 cm, for which conduction is the dominant heat transfer mode, in comparison to radiation in real pool fire scenarios or experiments[20,21]. Clearly, there is a lack of experimental data to the quantitative thermal hazard analysis and corresponding firefighting for transformer fire accidents.

To fill this knowledge gap, this work aims to experimentally investigate the transformer oil burning behaviors of pool fires using different pool diameters, mainly

in the radiation-controlled regime (D ⩾ 20 cm). The mass burning rate, flame height, liquid layer temperature, flame temperature and radiation are discussed and analyzed in detail. Furthermore, correlations of burning rate, flame temperature and radiation fraction are deduced based on the experiments, which will be of practical use in thermal hazard analysis of transformer oil fire accidents as well as corresponding firefighting.

2. EXPERIMENTAL SETUP

The overall schematic of the experimental setup is shown in Figure 1. All tests were conducted in a large hall. The doors and windows of the hall were all closed but not sealed during the tests, so the wind effect was not considered in this work. In the tests, KI25X transformer oil was used and the detail characteristics were shown in Table 1.

Table 1. The characteristics of KI25X transformer oil

Properties	Value
Density (kg/m^3)	883
Flash point (℃)	155
Heat conductivity (W/(m K))[19]	0.128
Heat capacity (J/(kg K))[22]	1960
Effective heat of combustion (MJ/kg)[6]	40

In total, six fuel pans were used having diameters of 20, 30, 40, 60, 80, and 100cm as shown in Table 2. The height of the side wall of the pan is fixed at 10cm. In order to examine the effects of the fuel thickness, three averaged fuel thicknesses (1cm, 3cm, 5cm) were used. A digital vernier caliper was used to measure the liquid layer thickness at different locations of the pan. The pan was placed on the top of a load cell (precision: 0.1g, maximum: 35 kg, Sartorius) to record the real time fuel mass. A fireproof board was placed between the load cell and the pan to protect the load cell.

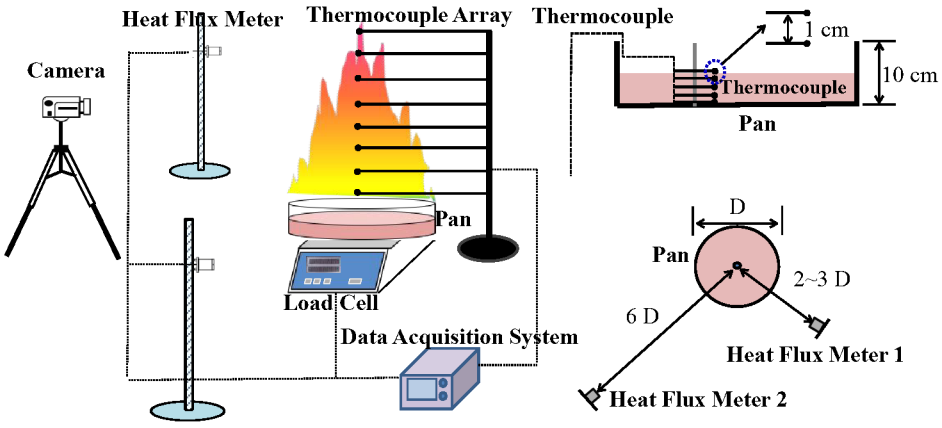

Figure 1. Schematic of experimental setup and the detail layout of thermocouples and heat flux meters

In the tests, both liquid temperature and flame temperature were measured. In order to measure the liquid temperature, a thermocouple (tip of 1mm, uncertainties ±1K) array was placed inside the pan at 1, 2, 3, 4, and 5 cm above the pan bottom surface (Figure 1). In addition, a set of 10 thermocouples (tip of 5mm, uncertainties ±5K) was used to measure the flame temperature and positioned evenly in the flame region above the pan in vertical direction at a 15cm interval.

Radiative heat flux was measured using two water-cooled heat flux meters (SBG 01) with a nearly hemispherical wide view angle (Figure 1). The maximum range of the heat flux meters is 50 kW/m^2 and the accuracy is more than 95%. In the analysis of radiative heat flux, there were two widely used models to calculate the distributions of heat flux surrounding a fire source, namely Source flame model and Solid flame model[24,25]. Therefore, one heat flux meter was positioned near the pan (L<5D) and the other one about six times of the pool diameter measured from the center of the pool fire (>5D). Two cameras with a sampling frequency of 25 fps were positioned at 8 m horizontally away from the pool fire center from different directions to record the flame shape, based on which the flame height is deduced.

The indoor temperature was 28 ± 3°C and the humidity remained at around 56 ± 10% during the tests. The specification of the test conditions are shown in Table 2. Tests with an averaged thickness of 5 cm were not conducted for some large pan diameters due to the measuring limitation of the balance. However, as it will be

shown in the results, the steady burning rate is independent of the fuel thickness when the fuel thickness is more than 1 cm. For ignition, 10 mL heptane was injected into the pan and ignited using a butane hand torch to initiate the combustion of the transformer oil.

Table 2. Specification of the test conditions

No.	Diameter (cm)	Averaged thickness (cm)	Mass (g)	No.	Diameter (cm)	Averaged thickness (cm)	Mass (g)
1	20	1.0	407	9	40	5.0	5576
2	20	3.0	845	10	60	1.0	2586
3	20	5.0	1419	11	60	3.0	7540
4	30	1.0	647	12	60	5.0	12530
5	30	3.0	1818	13	80	1.0	4540
6	30	5.0	3174	14	80	3.0	13390
7	40	1.0	1253	15	100	3.0	20830
8	40	3.0	3396				

3. RESULT AND DISCUSSION

3.1 Burning rate

The transient burning rates of selected tests with different initial thicknesses are shown in Figure 2. The whole burning process can be divided into four distinctive stages: (a) ignition stage, (b) increasing burning rate stage, (c) steady burning stage and (d) extinguishment. At the ignition stage, it was observed that the flame only covered part of the fuel surface and the flame gradually spread to the whole surface. During this period, most of the transformer oil was not ignited and the flame was mainly due to the heptane burning. At the second stage, the burning rate increased quickly, accompanied by a quick increase of the flame height. The flame detached from the surface of the fuel due to limited availability of oxygen in the pan. Meanwhile, black smoke was gradually observed in this stage. At the steady burning stage, the burning rate and the flame height are nearly constant for a relatively long

period of time. In this period, the heat feedback from the flame to the fuel surface and the heat transfer process are nearly constant. At the last stage, the flame re-entered the pan and disappeared in a short time. The detailed characteristics in each stage are shown in Figure 3.

Figure 2 shows that the steady burning rate for tests with the same pool diameter is nearly constant, independent of its initial thickness in the tests. For example, for the 20 cm cases the steady burning rate is 12.69, 12.34 and 12.18 g/(m^{2}s) for the initial thickness of 1 cm, 3cm and 5cm respectively and the maximum relative difference is less than 5%. Subsequently, the fuel thickness effects on the steady burning rate are not considered and the averaged burning rate is used for further analysis.

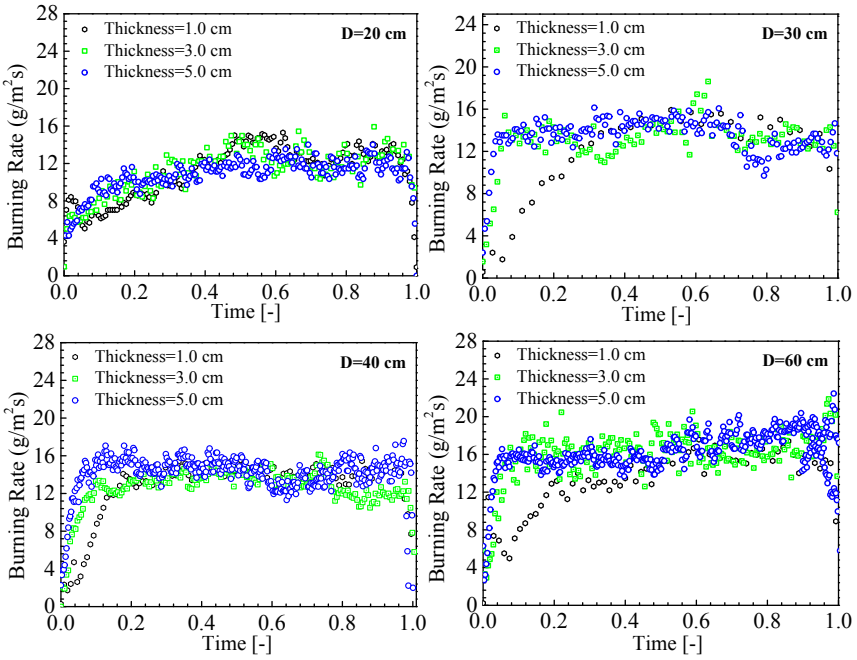

Figure 2. Experimental data of burning rate for different initial thickness with varied diameter (Time[-]=T_{real}/T_{total})

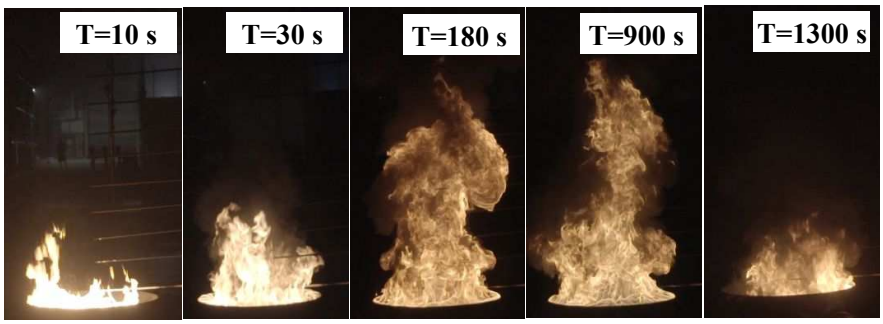

Figure 3. The burning process pictures of Test-14

Figure 4 plots the average steady burning rate as a function of pool diameter. Previous experimental data for transform oils with different pool diameters (1.2 m and 1.7 m) by Heskestad[10] and Kung and Stavrianidis[12] are also included along with the correlation proposed by Burgess [11] for comparison purpose.

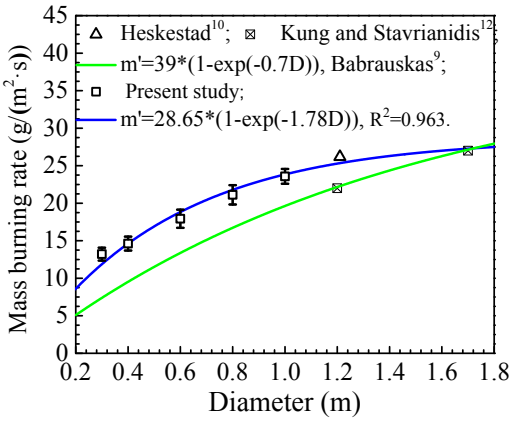

Figure 4. The mass burning rate as a function of burning diameter

The experimental data show that the burning rate increases with increasing pool diameter and approaches a constant value for large diameters. This trend is consistent with that of other hydrocarbon fuels[7-8]. For a pool fire, the total feedback heat from the flame to the fuel surface controls the burning rate and can be expressed as:

$$q_f = \frac{4k(T_r - T_l)}{D} + h(T_g - T_l) + \sigma F(T_f^4 - T_l^4)(1 - \exp(-k'D)) \quad (1)$$

where k, h and σ represents heat conduction coefficient, the convective heat transfer coefficient, and Stefan–Boltzmann constant, respectively; k' is in a constant which equals the extinction coefficient multiplied by the mean beam length corrector ($k\beta$); D is the pool diameter, F is the view factor, and T_r ,T_g, T_f and T_l are the temperatures of the pool rim, liquid gas above the liquid surface, flame and liquid fuel, respectively. For radiation-controlled burning (D>20cm)[7], the heat feedback can be simplified as:

$$q_f = \sigma F(T_f^4 - T_{boil}^4)(1 - \exp(-k'D)) \quad (2)$$

The burning rate (m') can be written as

$$m'(c_p(T_{boil} - T_\infty) + L_v) = q_f \quad (3)$$

where c_p is the specific heat at constant pressure, L_v is the latent heat of vaporization, and T_{boil} and T_∞ are the fuel boiling point and ambient temperature, respectively. Combining eqs (1-3), the burning rate can finally be expressed as:

$$m' = \frac{\sigma F(T_f^4 - T_l^4)}{c_p(T_{boil} - T_\infty) + L_v}(1 - \exp(-k'D)) = m''_\infty(1 - \exp(-k'D)) \quad (4)$$

where m''_∞ is the mass burning rate of a pool fire with an infinite pool diameter. The burning rate of most fuels with diameter larger than 1m can be approximated as the maximum burning value (m''_∞)[9]. In this study, the parameters of m''_∞ and k' are obtained based on the experimental data fitting as was done in the paper[9], as shown in Figure 3. The present correlation also agrees with the other tests with different pool diameters (Diameter: 1.2 m, 1.7 m) in the references[10,12].

3.2 Flame height

Flame height associated with the heat flux distribution is a key parameter in pool fire thermal hazard analysis[8,11,14]. The flame height can be determined by means of the visible images obtained from the video recordings. In the tests, the two cameras were located far away from the pool at different positions. An algorithm was developed to distinguish the flame contour. Videos of the flames were converted to a series of binary pictures and then the flame height was be determined based on a certain scale, as commonly done in literatures[26-28]. The detailed processing examples are shown in Figure 5.

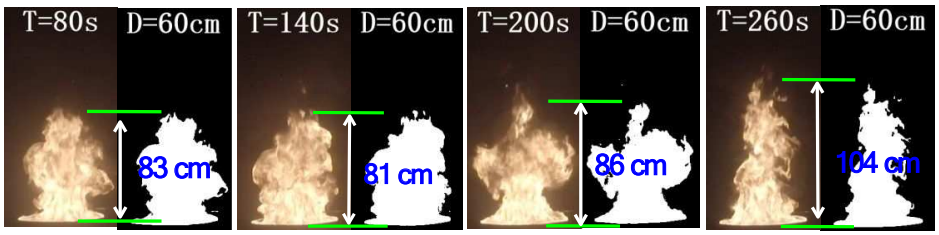

Figure 5. Flame contour extraction map

After obtaining the instantaneous flame heights in each picture, the flame intermittency was then obtained following the procedure in the paper[29]. Figure 6 presents the flame intermittency versus dimensionless height, *L/D*, for the case with a pool diameter of 0.8 m. The average flame height is the one having a flame intermittency of 0.5.

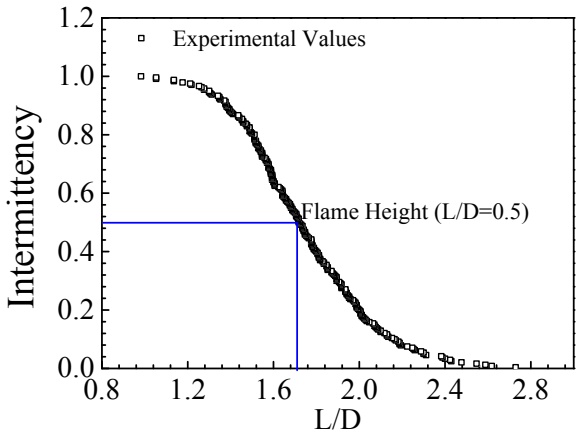

Figure 6. Flame height intermittence versus *L/D* for a diameter of 0.8 m burning (151s <t< 161 s)

The dimensionless flame height (*L/D*) can be correlated to a dimensionless number $\dot{Q}^*$ [30-33] as.

$$L/D = a(Q^*)^b + c \quad (5)$$

The parameters of *a*, *b* and *c* are constants, which are given in Table 3. It can be seen that their values vary significantly, because they are determined based on different tests having a wide range of scales and using different kinds of fuels.

Table 3. The parameters used to evaluate the experimental flame length data

Parameters	Q^*	a	b	c	Note
Moorhouse[30]	$\frac{m'}{\rho_\infty\sqrt{gD}}$	4.7	0.21	0	Pool-fire: 12.2×15.4 m
Mangialavori and Rubino[31]	$\frac{m'}{\rho_\infty\sqrt{gD}}$	31.6	0.58	0	Pool diameter: 1–6 m
Fay[32]	$\frac{m'}{\rho_\infty\sqrt{gD}}$	15.5	0.4	0	LNG pool fires
McCaffrey[33]	$\frac{m'\Delta H_c\pi}{4\rho_\infty c_\infty T_\infty\sqrt{gl}}$	3.7	0.4	-1.02	Laboratory-scale data

Figure 7 shows a comparison of the present experimental flame heights and predictions using different correlations. As it can be seen in Figure 6, the predictions vary widely between different models. In the experimental data, we also included an

additional measurement for a pool dimeter of 1.9 m. The test was conducted to study fire suppression, but a steady flame height was observed before the fire extinguishing.

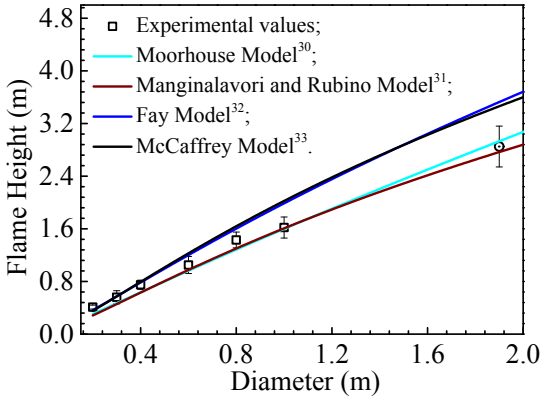

Figure 7. Comparison between the experimental flame height and the predictive values by different models

Figure 7 shows that the Fay's and McCaffrey's correlations can provide a good prediction when the pool diameter is small ($D \leqslant 40$cm). With the increase of pool diameter, both methods tend to overestimate the flame height. As we have known that the burning efficiency will gradually decrease for heavy oils burning due to the incomplete combustion. In addition, the production of strong smoke also limits the increase of flame with the increase of pool diameter. The Fay correlation is based on the LNG pool fire tests[32] and McCaffrey's correlation is from light fuels[33]. Therefore, the effects caused by burning efficiency and smoke on flame height are not considered adequately in the two correlations. With increasing burning diameter, both Moorhouse's and Mangialavori's correlations, derived from large scale pool fire tests, are in good agreement with the measurements. The average relative difference between the Moorhouse's and Mangialavori's correlations and the experimental data is similar, 0.114 and 0.120 respectively. This result is consistent with the finding of the paper[26] that Moorhouse's model is more suitable for large scale gasoline and diesel pool fire.

3.3. Temperature profile

3.3.1. Liquid and vapor temperature

For the temperature profile in a liquid layer, a uniform temperature layer near the

liquid surface and a lower layer with a large temperature gradient were observed for small pool fires (D=10 cm)[20-21,34]. However, there is still very limited information on the temperature profile in transformer oil burning, particularly for medium-scale (D>0.2m) pool fires. Figure 8 shows the results of the measured transient liquid temperature for selected cases.

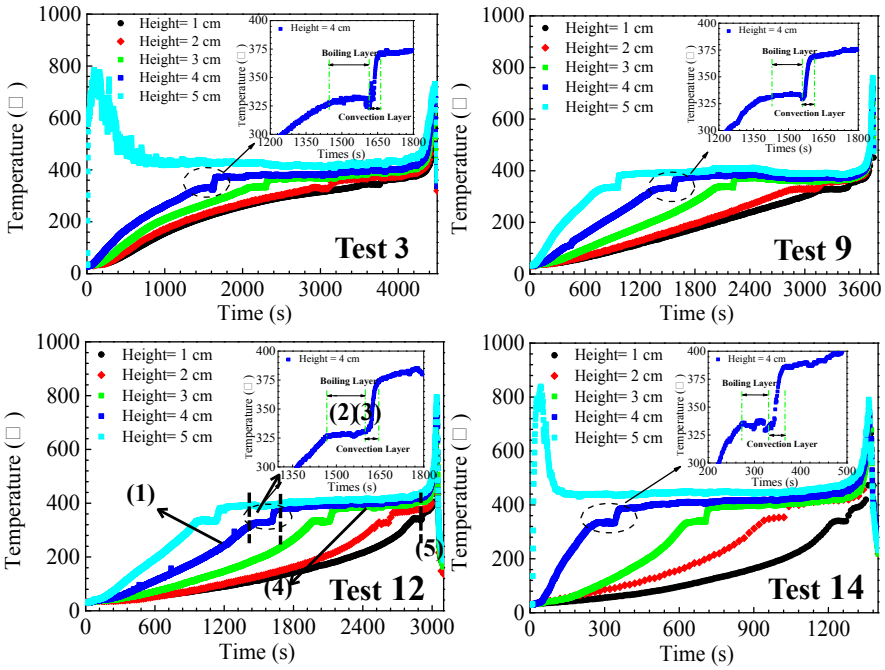

Figure 8. The measured temperature in the pan as a function of time

We recall that the top thermocouple in the pan is positioned at 5cm from the pan bottom surface, so it was initially exposed in the air for Test 3 and Test 14. This explains the initial sharp increase of temperature at this location. With increasing burning rate, this thermocouple became gradually immersed in the fuel vapor and the corresponding measured temperature decreases with time and eventually became constant at about 400 °C, indicating the formation of fuel-rich core region above the fuel surface[35]. In order to directly reflect the whole temperature variation in the pan, the measured temperature by the thermocouple at the height of 4cm from the bottom surface in Test-12 is used as an example. At the initial stage, the thermocouple was immersed in the fuel and the temperature increased from 30 ℃ to 332 ℃. As the measured temperature achieved the boiling point, the measured value kept nearly constant from 1423s to 1565s. After 1565s, the measured temperature experienced a

quick increase and then remained nearly constant until near the end of the tests, when the temperature increased dramatically around from 400℃ to 800℃ indicating the presence of the flame at this location. According the temperature variation in the pan, this process can be divided into five stages, as shown in Figure 8 (Test 12). And the detailed characteristic in each stage is described as follows:

(1) Gradually temperature increase stage: After ignition, the surface temperature will achieve the boiling point in a short time[36]. The fuel below the boiling layer will be heated by heat conduction. Meanwhile, the distance between the thermocouple and the fuel surface will decrease with the continuous burning. So the measured temperature will increase until it reaches the boiling point.

(2) Steady temperature stage: The measured temperature is nearly constant (~330℃, the boiling temperature) when the measurement positions are close to the fuel surface. The measured temperature with the boiling point can keep constant and continue for some time until the thermocouple is exposed to the fuel vapor. The appearance of the steady temperature stage illustrates the existence of the boiling layer below the fuel surface. Based on the temperature measurements in the liquid layer, the thickness of the boiling layer can be estimated as:

$$h_{boil} = w(t) \times (t_2 - t_1) \quad (6)$$

where w is the burning rate (mm/s), t_1 is the start time when the measured temperature achieves the boiling point and t_2 is the end time, after which the temperature exceeds the boiling point, followed by a quick temperature increase. Based on eq 6, the boiling thickness at different pool sizes (D=20cm, 40cm, 60cm, 80cm) is calculated and the average values are approximately 2.46 mm, 2.85 mm, 2.64 mm and 2.54mm, respectively, all slightly less than 3.0mm observed in the paper[21]. The reason for the deviation is closely associated with the radiation absorption properties of the fuel layer[20-21, 34].

(3) Sharp temperature increase stage: After the thermocouple is exposed to the fuel vapor, a sharp temperature increase from around 330℃ to 380℃ is observed. This illustrates the existence of a vapor layer with a large temperature gradient just above the fuel surface, which promotes the heat convection heat feedback between the fuel

and vapor.

(4) Second steady temperature stage: It has been known that there is a fuel-rich core region above the fuel surface for pool fires[35]. As the liquid fuel is vaporized and the surface of the fuel recedes, the thermocouples become immersed in the fuel vapor and not directly in contact with the flame. The speed at which the fuel surface decreases is very small, so it has little influence on the flame behavior. Therefore, the temperature of fuel vapor near the fuel surface in the pan can keep steady. The temperature increase at 4mm is only about 26 ºC at the start and the end of this stage. The slight increase is likely due to the small increase in the distance between the thermocouple and the fuel surface.

(5) Second sharp temperature increase stage: Near the end of burning, the liquid fuel is nearly all consumed and all the thermocouples were exposed in the vapor. The flame entered the pan where unburn gas vapor is, and as a result the measured temperature all increased sharply. The extinguishment of the flame followed shortly, indicated by the sudden decrease of the measured temperature.

3.3.2. Flame temperature

Figure 9 shows the axial flame temperature variations with time for Tests 4 and 15. The maximum value of flame temperature is about 800 ℃, with similar values observed in other tests. The variation of the flame temperature with time is consistent with that of the burning rate. For further analysis, the average temperature at the steady burning stage is used to study the vertical temperature profile.

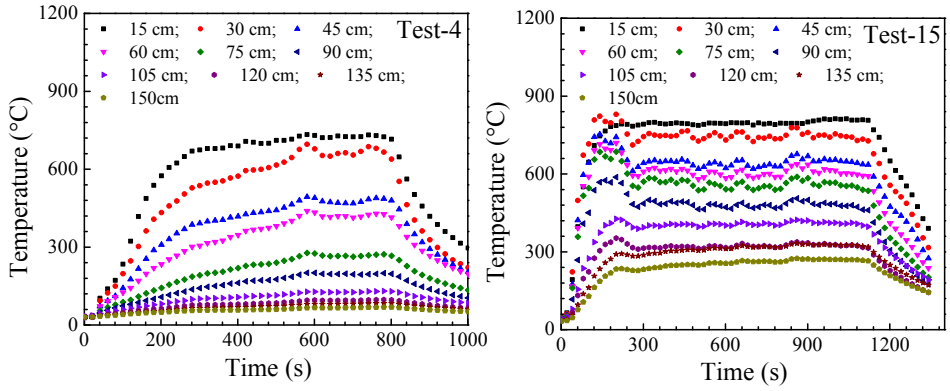

Figure 9. The axial flame temperature as a function of time

The dimensionless temperature increase,$(T_z - T_\infty)/T_\infty$, are plotted in Figure 9 against the normalized height, $Z/\dot{Q}^{0.4}$, where T_z is the flame temperature at location Z; T_∞ is the ambient temperature; The heat release rate ($\dot{Q}$) can be expressed as:

$$\dot{Q} = \mathrm{m}' \times \Delta H_c \times S \tag{7}$$

where S is the pool area ($\pi D^2/4$) and ΔH_c is the effective heat of combustion given in Table 1.

The flame temperature profile can be divided into three regions: isothermal zone; rapid decrease zone and slow decrease zone based on the temperature variation in some papers [37-39]. For example, a piecewise function is correlated and given by Tao et al. derived from the large scale aviation kerosene pool fire[37] as also shown in Figure 10.

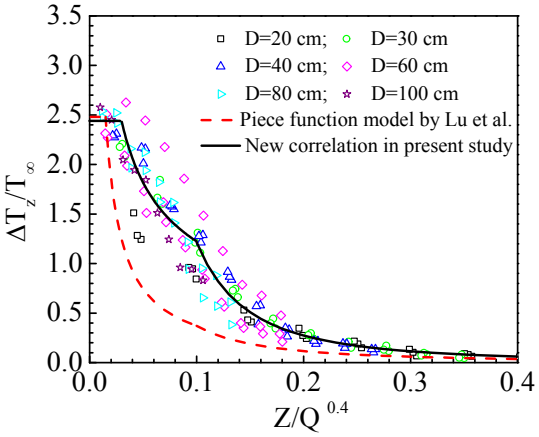

Figure 10. the normalized temperature rise $\Delta T_z/T_\infty$ as a function of $Z/Q^{2/5}$

It can be found that the modified model by Lu et al. gives a better agreement for the isothermal zone, while the deviation gradually becomes large for the second zone. This can be attributed to the difference in the pool diameter and fuel types. Base on the present experimental data, a new piecewise function can be deduced and the results are shown in Figure 9.

$$\frac{\Delta T_z}{T_\infty} = \begin{cases} 2.45; & Z/\dot{Q}^{0.4} < 0.03 \\ 0.33 \times (Z/\dot{Q}^{0.4})^{-0.57}; & 0.03 \le Z/\dot{Q}^{0.4} \le 0.1 \\ 0.0086 \times (Z/\dot{Q}^{0.4})^{-2.15}; & Z/\dot{Q}^{0.4} > 0.1 \end{cases} \tag{8}$$

It is noted in Figure 10 that the zone of the isothermal zone is narrow and the flame temperature decreases quickly in the second zone. The larger air entrainment and the

production of strong smoke results in the quick temperature decrease, which has been confirmed and discussed in the paper[37]. Here, it is important to emphasize that the three zones in eq 8 don't correspond completely to the traditional three flame regions (i.e., continuous, intermittent and plume) but they provide a more accurate temperature prediction.

3.4. Radiation

3.4.1 Radiation fraction

The primary hazard of transformer oil pool fires is the thermal impact by radiation to the nearby equipment. The flame radiation fraction is a key parameter to determine radiative heat flux distribution and can be calculated by the point source method as described in some references [40-42].

$$X_r = \frac{\dot{Q}_r}{\dot{Q}_t} = \frac{4\pi R^2 q''_r}{m'S\,\Delta H_c} \tag{9}$$

where $\dot{Q}_r$ is the total emitted radiation from the flame, $\dot{Q}_t$ is the total energy of burning, q''_r is the measured radiative heat flux, R is the distance from the vertical flame mid-height point to a target. This method is based on the assumption that all radiation emits from a point and this is valid on the condition that the distance between the target and flame is far enough[41]. In practical calculations, the separation distances more than five pool radii will be accepted[41-42]. The detailed schematic of this method is shown in Figure10. The measurements of the heat flux meter positioned at a distance about six times of the pool diameter in the tests were used in the calculations. The measurement of radiative heat flux of Tests 3, 10, 12 and 14 are shown in Figure 12.

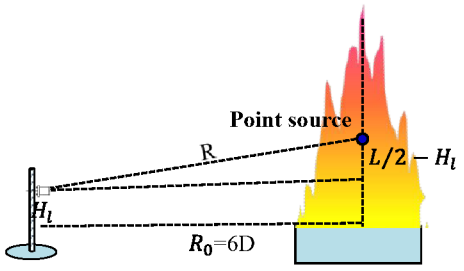

Figure 11. Calculation of flame radiation fraction (X_r) based on the single point model

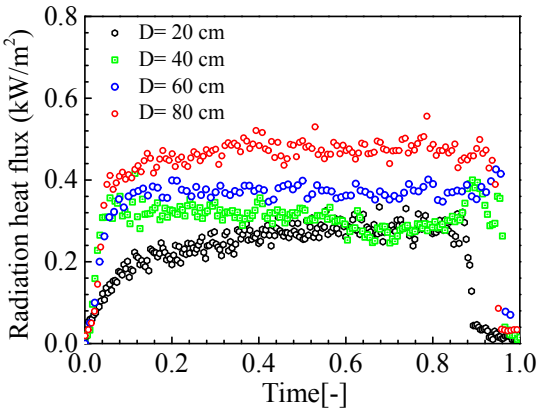

Figure 12. Measured radiative heat flux for different pool sizes (Time[-]=t/t_{total})

The variations of radiative heat flux are consistent with those of the burning rate and the measured values are nearly constant in the steady burning stage. In order to determine the radiation fraction, the average radiative heat flux at the steady burning stage is used. Based on eq 10, the radiation fraction is calculated and the results are shown in Figure 13.

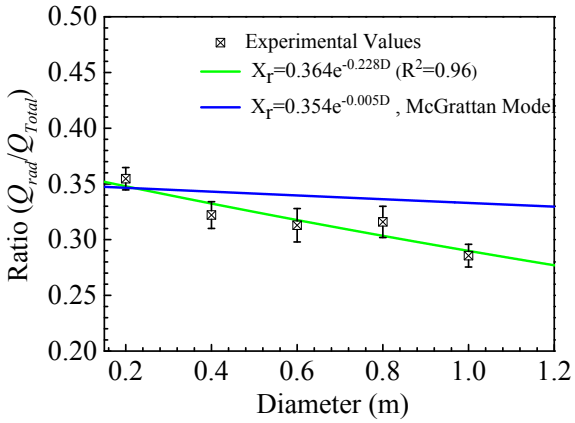

Figure 13. Experimental results vs. proposed model and McGrattan's model

The radiation fraction decreases with increasing pool diameter in Figure12, which is in accordance with the finding for other fuels[8, 26]. Existing correlations[8,23,43] for radiation fraction assume that X_r ~D$^{-0.5}$, ~constant, or an exponential relationship between X_r and pool diameter[42]. At present, McGrattan's model is widely used in some liquid pool fires [43-44].

$$X_r = X_{rmax} e^{-cD} \quad (10)$$

where $X_{rmax} = 0.35$ and c=0.05 [43]. Although these values are derived from the experimental data fitting, involving a range of different liquid fuels, there is still a large deviation for certain fuels, which has been illustrated by Chatris et al.[8]. In Figure 13, it can be seen that the predicted values by McGrattan model overestimates the practical values. So the parameters in eq 10 are reacquired ($X_{rmax} = 0.36$ and c=0.228) by the fitting of experimental date. The correlation coefficient can reach about 0.96. In the new correlations, the value of c is larger than the previous value, which means a quick decrease in radiation fraction with the increase of pool diameter. This is attributed to the obvious smoke blockage for the heavy oil burning as illustrated in Figure 14.

Figure 14. The smoke blockage effect on the flame radiation

3.4.2 Emissive power of flame surface

To calculate the radiative heat flux from a fire to a nearby object (at closer distances), a solid flame radiation model is widely used, in which the flame is idealized as a vertical cylinder emitting thermal radiation from its surface[44]. The radiative heat flux from a fire to a nearby object can be expressed as:

$$\dot{q}'' = F_{1-2}\tau E_f \quad (11)$$

where F_{1-2} is a geometric view factor; τ is the atmospheric transmissivity to thermal radiation, simplified as one for near target[45]; E_f is an average emissive power of flame surface. Various empirical models are available to predict emissive power and the corresponding calculation results in the tests are shown in Table 4. For Model 1, the average flame temperature obtained from the experiments, around 1030 K, is used for the calculation.

Table 4. The flame surface emissive power model

Model type	Correlations	Parameters	Results (kW/m²)
Model 1	$E = \sigma \varepsilon_f T^4$	$\sigma = 5.67 \times 10^{-8} W/(m^2 K^4)$ $\varepsilon_f = 1 - e^{-kD}$ [44]; T_f=1030K	**20~54**
Model 2 [46]	$E = E_{max} \times 0.2 + E_{soot} \times 0.8$	$E_{max} = 130$ kW/m²; E_{soot}=20 kW/m²	**42**
Model 3 (Shokri and Beyler) [47]	$E = E_{max} \times 10^{-aD}$	$E_{max} = 58$ kW/m², a=0.00823 m⁻¹	**56.9~57.8**
Molde 4 (Mudan and Croce) [48]	$E = E_{max} e^{-sD} + E_s(1 - e^{-sD})$	E_{max}=140 kW/m²; E_s=20 kW/m²; s=0.12 m⁻¹.	**126~137**
Model 5 [44-45]	$E = X_r \dot{Q}_{total}/A$	$X_r = 0.36e^{-0.027D}$; A=πDH;	**22~35**

The view factor F_{1-2} is a geometric parameter, defined as eq 12. The schematic of radiation transfer between flame and target is shown in Figure 15.

$$F_{12} = F_{A_1 \to A_2} = \frac{1}{A_1} \int_{A_2} \int_{A_1} \frac{\cos(\theta_1)\cos(\theta_2)}{\pi r^2} dA_1 dA_2 \quad (12)$$

where A_1 and A_2 are the area of the flame and the target, respectively and r is the distance from the flame surface to the target. The detailed meaning of parameters is shown in Figure 14(a). In this work, the method developed by Mudan[46] (the detailed process is shown in Appendix A) is used for calculating the view factor.

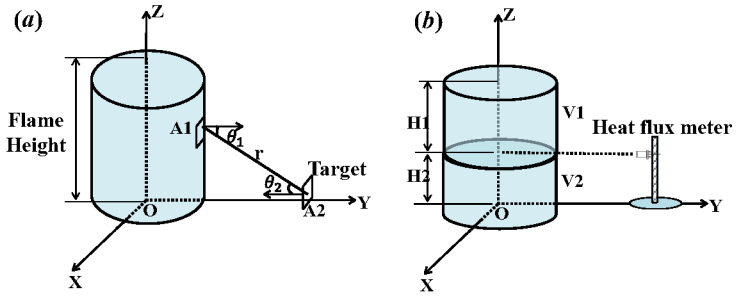

Figure 15. The schematic of heat radiation transfer between flame and target

The measured radiative heat flux by the near heat flux meter (2~4D) is used to examine the emissive power models given in Table 4. In the experimental setup, the heat flux meter kept a certain distance from the ground and the flame volume is divided into two parts, shown in Figure 14(b). In the tests, the measured average radiative heat flux at the steady burning phase nearly kept the same, independent of

the initial fuel thickness. So, the measured radiative heat flux values from tests 3, 6, 9, 12, 14 and 15 are used. The comparison between the experimental values and the calculations by different models is shown in Figure 16.

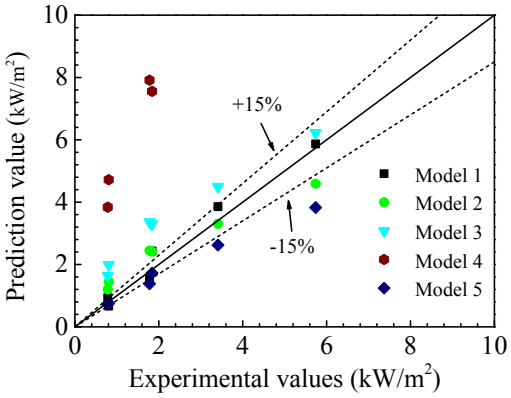

Figure 16. Comparison of experimental and calculated radiative heat flux using the different emissive surface models

It is seen that Model 1 can predict well the radiative heat flux within errors of ± 15%. For the small pool diameter burning (D≤40 cm), Model 5 can give a good prediction. However, the discrepancy increases with increase pool diameter. This could be attributed to the assumption that the flame is a perfect cylinder, while in fact necking-in due to the air entrainment occurs as shown in Figures 4 and 12, which has been discussed in detail in the paper[49]. The assumption in Model 5 results in a lower emissive power. Model 2 is recommended by Mudan for hydrogen fuels [44], and the predictive accuracy is relatively poor due to use of a constant for the emissive power. In Models 3 and 4, the predictive values are larger than the experimental values because the effects of smoke are not considered well since light component fuels were used in the development of these models. Overall, Model 1 ($E = \sigma \varepsilon_f T^4$) provides the best agreement and could be used to estimate the thermal radiation of pool fire on the surrounding objects in the actual fire accidents.

4. CONCLUSION

This study was aimed at identifying the burning characteristics of the transformer oil pool fires. To this end, a series of transformer oil pool fires was performed with different pool diameters. The burning rate, flame height, the liquid layer and flame

temperature profile, and radiation were measured and analyzed. The main results are as follows:

- New key burning parameters ($m''_\infty = 28.65$ g/m^2 and k'=1.78 m^{-1}) for the transformer oil pool fires are deduced based on present experimental data and also verified by existing data in the literature.
- Several empirical models for flame height were examined and it was found that the ones developed for heavy fuels agree better the measurements for transformer oils, which is consistent with the finding in Muñoz et al.'s study for a diesel pool fire.
- In the liquid layer, a boiling layer and a gradient layer were observed based on the temperature measurements. The average thickness of the boiling layer in the steady burning stage is approximately 2.6 mm for the transformer oil pool fires.
- A new piecewise function is provided to calculate the axial temperature for transformer oil pool fires, with a similar finding reported in the literature for aviation kerosene pool fires.
- Correlations are also developed for radiation fraction and flame surface emissive power. The radiation fraction is determined by the source model and a new correlation for the radiation fraction as a function of pool diameter ($X_r = 0.36e^{-0.228D}$) is deduced. Using the solid flame model, a flame emissive model based on the flame temperature ($E = \sigma\varepsilon_f T^4$) is found to estimate well the radiative heat flux of pool fire on the surrounding objects in transformer oil pool fire accidents.

The measurements reported here can help to enrich the basic experimental data of transformer oil pool fires which have been rarely reported. These results and fundamental analysis will lay a solid foundation of thermal hazard assessment for practical transformer oil fire accidents.

AUTHOR INFORMATION

Corresponding Author

*Tel: 86-15210567787. E-mail: 15210567787@163.com

Notes

The authors declare no competing financial interest.

ACKNOWLEDGEMENTS

This study was sponsored by the National Key R&D Program of China（No. 2018YFC0809900）,the National Natural Science Foundation of China (No. 51906253) and the Opening Funds of State Key Laboratory of Building Safety and Built Environment and National Engineering Research Center of Building Technology (BSBE 2017-03).

REFERENCES

(1) Wang, M.; Vandermaar, A.; and Srivastava, K. D. Review of condition assessment of power transformers in service. *Ieee. Electr. Insul. M.* **2002**, 18, 12-25.

(2) Dumitran, L.M.; Setnescu, R.; Notingher, P.V.; et al. Method for lifetime estimation of power transformer mineral oil. *Fuel* **2014**, 117, 756-762.

(3) Working Group A2.33. Guide for transformer fire safety practices. Paris, France: CIGRE, 2013.

(4) Zhao, Z.; Xu Y.; Wang J.; et al. Research on the fire safety of large power transformer. *High Voltage Engineering* **2015**, 41(10), 3378-3384.

(5) Xianji China 2019. Jinan 1000 kV UHV substation detonation caused 1 death and 2 injuries. https://www.xianjichina.com/special/detail_433103.html.

(6) Zhang, B.; Zhang, J.; Huang, Y.; et al. Burning process and fire characteristics of transformer oil. J. *Therm. Anal. Calorim.* **2019**, 7,1-10.

(7) Hamins, A.; Fischer, S.; Kashiwagi, T.; et al. Heat feedback to the fuel surface in pool fires. *Combust. Sci. Technol.* **1994**, 97(1-3), 37-62.

(8) Chatris, J.M.; Quintela, J.; Folch, J.; et al. Experimental study of burning rate in hydrocarbon pool fires. *Combust. Flame* **2001**, 126(1-2), 1373-1383.

(9) Babrauskas, V. Estimating large pool fire burning rates. *Fire Technol.* **1983**, 19(4), 251-261.

(10) Heskestad, G. Luminous heights of turbulent diffusion flames. *Fire Safety J.* **1983**, 5(2), 103-108.

(11) Burgess, D.S.; Strasser, A.; Grumer, J. Diffusive burning of liquid fuels in open trays. *Fire Res. Abstr. Rev.* **1961**, United States.

(12) Kung, H.C.; Stavrianidis, P. Buoyant plumes of large-scale pool fires. *Combustion Inst*. **1982**, 19(1), 905-912.

(13) Rew, P.J.; Hulbert, W.G.; Deaves, D.M. Modelling of thermal radiation from external hydrocarbon pool fires. *Process Saf. Environ.* **1997**, 75(2), 81-89.

(14) Sun, H.; Wang, C.; Liu, H.; et al. Experimental study of combustion characteristics of circular ring thin-layer pool fire. *Energy Fuels* **2017**, 31(9), 10082-10092.

(15) Sharma, A.; Mishra, K. Experimental set-up to measure the maximum mass burning rate of storage tank fires. *Process Saf. Environ.* **2019**, 131, 282-291.

(16) Zukoski, E.; Kubota T.; Cetegen, B. Entrainment in fire plumes. *Fire Safety J.* **1981**, 3(3), 107-121.

(17) Kim, S.C.; Lee, K.Y.; Hamins, A. Energy balance in medium-scale methanol, ethanol, and acetone pool fires. *Fire Safety J.* **2019**, 107:44-53.

(18) Zhang, B.; Zhang, J.; Wang, L.; et al. Investigation on effects of thickness on ignition characteristics and combustion process of the oil-impregnated transformer insulating paperboard. *J. Therm. Anal. Calorim.* **2018**, 132(1), 29-38.

(19) Wang, X.; Zhu, P.; Xu, H.; et al. Experimental study on the autoignition characteristics of pure and oil-impregnated transformer insulating paper board. *J. Therm. Anal. Calorim.* **2017**, 127(3), 2489-2497.

(20) Zhao, J.; Huang, H.; Jomaas, G.; et al. Experimental study of the burning behaviors of thin-layer pool fires. *Combust Flame* **2018**, 193, 327-334.

(21) Suo-Anttila, J.M.; Blanchat, T.K.; Ricks, A.J.; et al. Characterization of thermal radiation spectra in 2 m pool fires. *Combustion Inst.* **2009**, 32(2), 2567-2574.

(22) Hasan, M.I.; Improving the cooling performance of electrical distribution transformer using transformer oil–Based MEPCM suspension. *Int. J. Eng. Sci.* **2017**, 20(2), 502-510.

(23) Yang J.; Hamins, A.; Kashiwagi, T. Estimate of the effect of scale on radiative heat loss fraction and combustion efficiency. *Combust. Sci. Technol.* **1994**, 96(1-3),

183-188.

(24) Koseki, H. Large scale pool fires: results of recent experiments. *Fire Safety Sci.* **2000**, 6, 115-132.

(25) Hu, L.; Hu, J.; de Ris, J.L. Flame necking-in and instability characterization in small and medium pool fires with different lip heights. *Combust Flame* **2015**, 162(4): 1095-1103.

(26) Muñoz, M.; Arnaldos, J.; Casal, J.; et al. Analysis of the geometric and radiative characteristics of hydrocarbon pool fires. *Combust Flame* **2004**, 139(3), 263-277.

(27) Zhang, P.; Tang, X.; Tian, X.; et al. Experimental study on the interaction between fire and water mist in long and narrow spaces. *Appl. Therm. Eng.* **2016**, 94, 706-714.

(28) Wang, Q.; Tang, F.; Liu, H.; et al. Experimental Investigation on the effect of a reduced pressure on the combustion characteristics and flame height of gaseous fuel jets in parallel sidewalls. *Energy fuels* **2018**, 32(2), 2490-2496.

(29) Zukoski, E.; Cetegen, B.M.; Kubota, T. Visible structure of buoyant diffusion flames. *Combustion Inst.* **1985**, 20(1), 361-366.

(30) Moorhouse, J. Scaling criteria for pool fires derived from large-scale experiments. The Assessment of Major Hazards, Symposium Series **1982**, 71, 165-179.

(31) Mangialavori, G.; Rubino, F. Experimental tests on large hydrocarbon pool fires. *7th Int. Symp. on Loss Prevention and Safety Promotion in the Process Industries* **1992**, Taormina, Italy, 4-8.

(32) Fay, J.A. Model of large pool fires. *J. Hazard Mater.* **2006**, 136(2), 219-232.

(33) McCaffrey, B.J. Momentum implications for buoyant diffusion flames. *Combust. Flame* **1983**, 52, 149-167.

(34) Vali, A.; Nobes, D.S.; Kostiuk, L.W. Transport phenomena within the liquid phase of a laboratory-scale circular methanol pool fire. *Combust Flame* **2014**, 161(4), 1076-1084.

(35) Joulain, P. The behavior of pool fires: state of the art and new insights. *Combustion Inst.* **1998**, 27(2), 2691-2706.

(36) Garo, J.P., Vantelon, J.P., Koseki, H. Thin-layer boilover: Prediction of its onset and intensity. *Combust. Sci. Technol.***2006**, 178(7), 1217-1235.

(37) Tao, Y.; Lu, K.; Chen, X.; et al. Experimental investigation on the temperature profile of large scale RP-5 aviation kerosene pool fire in an open space. *Fuel* **2020**, 264, 116852.

(38) Li, C.; Yao, Y.; Tao, Z.; et al. Influence of depressurized environment on the fire behaviour in a dynamic pressure cabin. *Appl. Therm. Eng.* **2017**, 125, 972-977.

(39) Zhou, Z.; Wei, Y.; Li, H.; et al. Experimental analysis of low air pressure influences on fire plumes. *Int. J. Heat Mass Tran.* **2014**, 70, 578-585.

(40) Hamins, A.; Klassen, M.; Gore, J.; et al. Estimate of flame radiance via a single location measurement in liquid pool fires. *Combust Flame* **1991**, 86(3), 223-228.

(41) Hu, L.; Wang, Q.; Delichatsios, M.; et al. Flame radiation fraction behaviors of sooty buoyant turbulent jet diffusion flames in reduced-and normal atmospheric pressures and a global correlation with Reynolds number. *Fuel* **2014**, 116, 781-786.

(42) Hankinson, G.; Lowesmith, B.J. A consideration of methods of determining the radiative characteristics of jet fires. *Combust Flame* **2012**, 159(3), 1165-1177.

(43) Yang, J.C.; Hamins, A.; Kashiwagi, T. Estimate of the effect of scale on radiative heat loss fraction and combustion efficiency. *Combust. Sci. Technol.* **1994**, 96(1-3),183-188.

(44) McGrattan, K.B.; Baum, H.R.; Hamins, A. Thermal Radiation from Large Pool Fires, NIST (National Institute of Standards and Technology) NISTIR 6546, **2000**.

(45) Sudheer, S; Prabhu, S.V. Measurement of flame emissivity of gasoline pool fires. *Nucl. Eng. Des.* **2010**, 240(10), 3474-3480.

(46) Mudan, K.S. Thermal radiation hazards from hydrocarbon pool fires. *Prog. Energ. Coumbust* 1984, 10(1): 59-80.

(47) Shokri, M.; Beyler, C.L. Radiation from large pool fires. *J. Fire. Prot. Eng.* **1989**, 1, 141-150.

(48) Mudan, K.; Croce, P. Fire hazard calculations for large open hydrocarbon fires, SFPE Handbook of Fire Protection Engineering, 1st ed., National Fire Protection Association, Quincy, Ma., Section 2, **1988**.

(49) Hu, L.; Hu, J.; de Ris, J.L. Flame necking-in and instability characterization in small and medium pool fires with different lip heights. *Combust Flame* **2015**, 162(4), 1095-1103.